Biochemical and Biophysical Research Communications 451 (2014) 402–407

Contents lists available at ScienceDirect

Biochemical and Biophysical Research Communications

journal homepage: www.elsevier.com/locate/ybbrc

Structure and flexibility of the thermophilic cold-shock protein of *Thermus aquaticus*

Bonghwan Jin, Ki-Woong Jeong, Yangmee Kim *

Department of Bioscience and Biotechnology, BMIC, Konkuk University, Seoul 143-701, South Korea

ARTICLE INFO

Article history:
Received 21 July 2014
Available online 4 August 2014

Keywords:
Cold-shock proteins
NMR spectroscopy
Structure
Backbone dynamics
Thermus aquaticus

ABSTRACT

The thermophilic bacterium *Thermus aquaticus* is a well-known source of Taq polymerase. Here, we studied the structure and dynamics of the *T. aquaticus* cold-shock protein (*Ta*-Csp) to better understand its thermostability using NMR spectroscopy. We found that *Ta*-Csp has a five-stranded β-barrel structure with five salt bridges which are important for more rigid structure and a higher melting temperature (76 °C) of *Ta*-Csp compared to mesophilic and psychrophilic Csps. Microsecond to millisecond time scale exchange processes occur only at the β1–β2 surface region of the nucleic acid binding site with an average conformational exchange rate constant of 674 s^{-1}. The results imply that thermophilic *Ta*-Csp has a more rigid structure and may not need high structural flexibility to accommodate nucleic acids upon cold shock compared to its mesophile and psychrophile counterparts.

1. Introduction

Many organisms have the ability to respond to changes in the environment, such as changes in temperature, pressure, osmotic conditions, and oxygen availability. Bacteria have evolved specific physiological mechanisms to help them adapt to temperatures lower than their optimal growth temperatures. The adaptation of bacteria to minimal growth temperature is reflected by changes in the growth rate, levels of fatty acid saturation, and the regulation of DNA, RNA, and protein synthesis in the cells [1]. At minimal growth temperature, synthesis of most proteins is downregulated, while that of cold-shock proteins (Csps) is upregulated [2].

Csps are found in a wide range of bacteria, including psychrophilic, mesophilic, thermophilic, and hyperthermophilic species. They share a highly conserved sequence and structure. Csps function as RNA chaperones, assisting the unfolding of mRNAs [3,4]. The three-dimensional structures of several Csps have been resolved by X-ray crystallography and nuclear magnetic resonance (NMR) spectroscopy. These include the following: mesophilic Csps, such as those of *Escherichia coli* (*Ec*-CspA) [5,6], *Bacillus subtilis* (*Bs*-CspB) [7–9], *Salmonella typhimurium* (*St*-Csp) [10], *Mycobacterium tuberculosis* (*MTB*-Csp) [11], and *Rickettsia rickettsia* (*Rr*-Csp) [12]; thermophilic Csps, such as the *Bacillus caldolyticus* Csp (*Bc*-Csp) [13,14] and *Thermotoga maritima* Csp (*Tm*-Csp) [15]; and a psychrophilic Csp, the *Listeria monocytogenes* CspA (*Lm*-CspA) [16]. All of these Csps contain five antiparallel β-strands with an oligonucleotide-binding fold. Aromatic residues located in two of these conserved nucleic acid binding motifs, ribonucleoprotein (RNP) 1 and RNP 2, facilitate binding with single-stranded nucleic acids.

Csps from thermophilic bacteria with known 3D structures are *Bc*-Csp from the *B. caldolyticus* and *Tm*-Csp from the hyperthermophilic bacteria *T. maritima*. Both Csps have higher thermal stability than their mesophile and psychrophile counterparts. However, motional properties of thermophilic Csps have not been studied by spin relaxation experiment, yet.

Thermus aquaticus is a species of thermophilic bacteria that thrives at 70 °C, but can survive at temperatures ranging from 50 °C to 80 °C. It is the source of the Taq DNA polymerase widely used for DNA amplification in the polymerase chain reaction technique. Here, we determined the solution structures of free *Ta*-Csp and the single-stranded nucleic acid [heptathymidine (dT_7)]-bound complex *Ta*-Csp-dT_7. For the first time, we investigated the structural flexibilities of *Ta*-Csp to understand the origin of the high thermostability of thermophilic Csps using spin relaxation experiment.

2. Materials and methods

2.1. Protein expression, isotopic enrichment, and purification

Expression of *Ta*-Csp, isotopic enrichment, and purification was performed as described previously [16]. Concentrated protein was purified using size-exclusion and hydrophobic-interaction

* Corresponding author. Fax: +82 2 447 5987.
E-mail address: ymkim@konkuk.ac.kr (Y. Kim).

http://dx.doi.org/10.1016/j.bbrc.2014.07.127
0006-291X/

chromatography. The protein yield from 1 L of cell culture was generally between 0.5 and 1 mg.

2.2. Circular dichroism measurement of Ta-Csp

Circular dichroism (CD) measurements were performed in a J810 spectropolarimeter (Jasco) using a cell with a 1-mm path length. The CD spectra of 50 μM *Ta*-Csp were measured at 0.1 nm intervals from 190 nm to 250 nm in 50 mM potassium phosphate buffer (pH 6.0) containing 100 mM KCl and 0.1 mM EDTA at 25 °C; data from 10 scans were averaged. CD data were expressed as the mean residue ellipticity (θ) in degrees square centimeters per decimole. Protein T_m values were determined from a series of CD spectra obtained at temperatures ranging from 15 °C to 100 °C.

2.3. NMR experiments and structure determination

All NMR experiments were performed as described previously [16] at 25 °C on a Bruker Avance 500 and 800 MHz spectrometer at the Korea Basic Science Institute. Nuclear Overhauser effect (NOE) distance constraints were measured from 3D $^{1}H–^{15}N$ and $^{1}H–^{13}C$ nuclear Overhauser effect spectroscopy–heteronuclear single-quantum coherence (NOESY–HSQC) spectra acquired with an 800 MHz Bruker Avance NMR spectrometer equipped with a $^{1}H–(^{13}C,^{15}N)$ triple-resonance probe using a mixing time of 120 ms [17–19]. NMR spectra were processed with NMRPipe [20] and decoded with Sparky [21]. Structure calculations were performed using the CYANA 2.1 [22] together with dihedral (φ and ψ) constraints using the TALOS [23]. Final coordinates and NOE constraints have been deposited in the Protein Data Bank (PDB) as entries 2MO1 (*Ta*-Csp-dT_7) and 2MO0 (free *Ta*-Csp).

2.4. NMR investigation of backbone dynamics

We performed NMR spin-relaxation experiments on free *Ta*-Csp and dT_7-bound *Ta*-Csp (at a molar ratio of *Ta*-Csp to dT_7 of 1:1) and analyzed R_1, R_2, and heteronuclear NOE (hNOE) NMR spectra acquired on a Bruker Avance 500 MHz spectrometer [24]. Longitudinal (R_1) spin-relaxation rates were obtained, and relaxation delays were 0.00200 (measured twice), 0.0450, 0.100, 0.200, 0.315 (measured twice), 0.550, 0.800, and 1.00 s. The transverse (R_2) relaxation rate was measured with relaxation delays of 0 (measured twice), 0.0166, 0.0333, 0.0499 (measured twice), 0.0666, 0.116, 0.183, and 0.283 s. The heteronuclear cross-relaxation rate was obtained from NOE experiments by interleaving pulse sequences with and without proton saturation. The recycle delay and proton saturation time in hNOE measurements were 4.5 and 3.0 s, respectively. All relaxation spectra were acquired as described previously [16]. The data were processed with NMRPipe [20] and visualized using Sparky [21]. R_1, R_2, and hNOEs rates were determined as described in our previous paper [16,25,26]. Constant-time relaxation-compensated Carr–Purcell–Meiboom–Gill (CPMG) experiments [27] were performed at 500 MHz and 800 MHz spectrometer as described previously [16]. The intensities of cross-peaks were then converted into decay rates, R_2^{eff}, for a given field strength, υ_{cp} [28]. CPMG dispersion profiles were fit to a two-state exchange model using CATIA program from F. Hansen (http://pound.med.utoronto.ca/~flemming/catia).

2.5. Fluorescence quenching

Quenching of the intrinsic fluorescence of W8 in *Ta*-Csp upon binding to nucleic acids was used to determine binding constants. The binding constant of oligonucleotides was measured on a RF-5301PC spectrofluorophotometer. *Ta*-Csp protein (final concentration, 10 μM) was added to 50 mM potassium phosphate buffer containing 100 mM KCl and 0.1 mM EDTA at pH 6.0 at a final protein-to-oligonucleotide ratio of 1:10. The sample was placed in a 2 ml thermostatically controlled cuvette, and excitation and emission path lengths were set at 10 nm. The sample was excited at 290 nm, and emission spectra were recorded for light-scattering effects from 300 nm to 500 nm. Dissociation constants (K_d) were estimated as described previously [16].

3. Results

3.1. Thermostability of Ta-Csp and Ta-Csp-dT_7 determined through CD experiments

Csps from different species, ranging from psychrophilic to thermophilic bacteria, share high sequence as well as structural similarity. *Ta*-Csp showed 59% amino acid sequence identity with *Bc*-Csp, 56% with *Tm*-Csp, and 54% with *Bs*-CspB. Despite these structural similarities, they display dramatic differences in thermostability [29]. In order to better understand the cold-shock response in bacteria, we explored structural characteristics that may potentially account for these differences in thermostability among Csps.

The secondary structures of *Ta*-Csp and *Ta*-Csp-dT_7 were investigated by CD measurements. As shown in Fig. 1A, CD spectra of *Ta*-Csp and *Ta*-Csp-dT_7 are very similar, showing a maximum at 200 nm and a minimum at 212 nm, characteristic of a β-sheet structure. Analysis of the thermal denaturation curves obtained at temperatures ranging from 15 °C to 100 °C showed the T_m of *Ta*-Csp to be 76 °C, indicating that *Ta*-Csp is much more thermostable than psychrophilic and mesophilic Csps.

3.2. Solution structures of Ta-Csp and Ta-Csp-dT_7

The three-dimensional structures of free *Ta*-Csp and *Ta*-Csp-dT_7 were calculated based on NMR constraints; NMR structural statistics for these calculations are summarized in Table 1. We included 979 and 978 conformational constraints in the structure calculation of free *Ta*-Csp and *Ta*-Csp-dT_7, respectively. The structures revealed that free *Ta*-Csp forms a Greek-key topology, a closed β-barrel consisting of 5 β-strands; 2 residues in these β-sheets (T5 and K64) form β-bulges, which break strand β1 into β1′and β1″and strand β5 into β5′ and β5″. As a result, two β-sheets surfaces—β-sheets 1 and 2—are formed by strands β1″–β2–β3 and β1′–β4–β5′–β5″. Five well-defined β-strands were identified in free *Ta*-Csp: β_1 (K2-N10), β_2 (Y15-Q20), β_3 (D25-H29), β_4 (H46-G54), and β_5 (P60-R67). They can be arranged into 2 antiparallel β-pleated sheets stabilized by hydrophobic interactions and hydrogen bond networks within the β-sheets. The side chain groups of V6, F9, I18, V26, V28, I33, L41, V47, F49, V51, A62, and V65 point to the interior of the β-barrel structure in *Ta*-Csp, forming a hydrophobic core. Flexible loop 3 is approximately 16 residues long, and loop 4 encompasses 5 residues from R55 to G59.

The structure of *Ta*-Csp-dT_7 is almost invariant compared to that of the free form, having exactly the same five β strands. As shown in Fig. 1B and C both the *Ta*-Csp structure and the structure of the complex displayed ionic interactions between various residues: E21-K3-E48-R66, K7-D25, and E52-K63. Fig. 1D shows the solvent-exposed hydrophobic residues such as W8, Y15, F17, F27, V28, F30, and F38 as well as the hydrophilic residues which form a cluster of protein surfaces and are important for binding to single-stranded nucleic acids [8,9]. The backbone root mean square deviations (RMSDs) between free *Ta*-Csp and dT_7-bound *Ta*-Csp for the 5 β strands and the 4 loops were measured to be 0.22 Å (β_1), 0.30 Å (β_2), 0.31 Å (β_3), 0.27 Å (β_4), 0.15 Å (β_5), 0.16 Å (loop 1), 1.10 Å (loop 2), 1.18 Å (loop 3), and 0.25 Å (loop 4). The backbone RMSD relative to the mean structure for all residues was

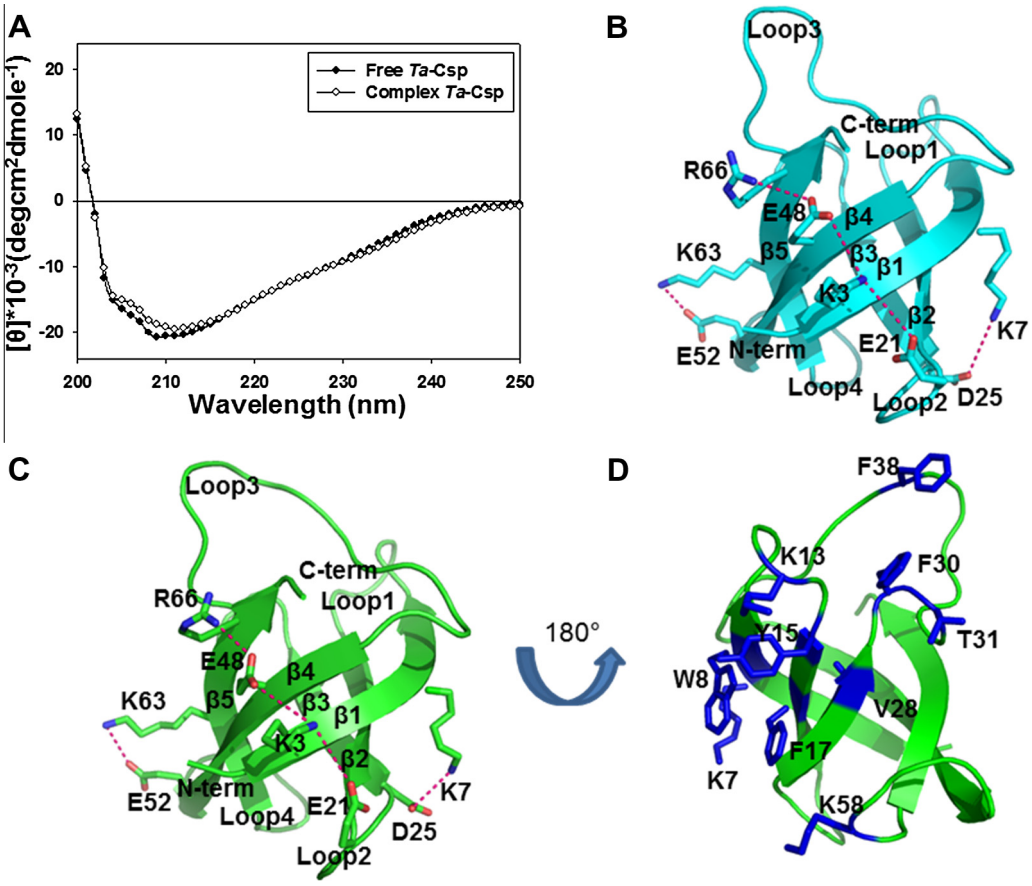

Fig. 1. (A) CD spectra of *Ta*-Csp (filled circles) and *Ta*-Csp-dT_7 (open circles) in 50 mM potassium phosphate containing 100 mM KCl and 0.1 mM EDTA (pH 6.0) at 25 °C. (B) Average NMR structures of free *Ta*-Csp (cyan) and (C) *Ta*-Csp-dT_7 (green) determined using NMR spectroscopy. Hydrogen bonds are represented by dotted lines. (D) Structure of *Ta*-Csp-dT_7 showing the side chains of dT_7 binding residues in blue. (For interpretation of the references to colour in this figure legend, the reader is referred to the web version of this article.)

Table 1
Structural statistics and mean pairwise root mean squared deviations for the 20 lowest-energy structures of *Ta*-Csp and *Ta*-Csp-dT_7.

Distance restraints	Free *Ta*-Csp	Complexed *Ta*-Csp
Total	979	968
Intraresidual and sequential	510	500
Medium-range	105	104
Long-range	364	364
Dihedral angle restraints	117	117
Hydrogen bonds	28	28
Rmsd of the backbone all residues (Å)	0.43 ± 0.20	0.39 ± 0.10
Rmsd from idealized geometry		
Bonds (Å)	0.0035 ± 0.00001	0.0035 ± 0.00002
Angle (°)	0.47 ± 0.019	0.46 ± 0.036
Water refinement energies (kcal mol^{-1})		
E_{NOE}	11.16 ± 11	14.16 ± 1
E_{cdih}	1.12 ± 0.006	1.71 ± 0.01
E_{elec}	−2653 ± 23	−2884 ± 24
E_{vdw}	−321 ± 3	−261 ± 6
E_{total}	−2536 ± 21	−2661 ± 22
Average violations		
Distance violation (0.50 Å < d)	0	0
Angle violation (θ > 5°)	0	0
Ramachandran plot statistics (%)		
Residues in most favored regions	75.7	77.5
Residues in additional allowed regions	23.4	22.4
Residues in generously allowed regions	0.9	0.1
Residues in disallowed regions	0	0

0.43 ± 0.20 Å for free *Ta*-Csp and 0.39 ± 0.10 Å for *Ta*-Csp-dT_7 (Table 1). In the β-sheet-ordered regions, backbone RMSD relative to the mean structure was 0.27 ± 0.02 Å for free *Ta*-Csp and 0.28 ± 0.01 Å for *Ta*-Csp-dT_7.

3.3. Chemical shift perturbations of Ta-Csp upon dT_7 binding

In order to investigate local structural rearrangements upon a ligand binding to the protein, chemical shift variations were analyzed by comparing the ^{15}N–^{1}H HSQC spectra of free *Ta*-Csp and *Ta*-Csp-dT_7. Fig. 2A shows the overlay of the two-dimensional ^{15}N–^{1}H HSQC spectra of *Ta*-Csp and dT_7-bound *Ta*-Csp at a *Ta*-Csp-to-dT_7 molar ratio of 1:1. Blue lines in Fig. 2A and B indicate residues showing larger chemical shift variations upon dT_7 binding more than 0.25 ppm. Large changes in chemical shift imply that most residues facilitate the binding of dT_7 through direct interaction between the base or phosphate group of dT_7 and the binding site, and also through conformational rearrangements of the flexible loop region away from the binding interface such as I33, L41 and G56. These binding residues are exactly the same to the nucleic acid binding residues in NMR and X-ray structures of *Bs*-CspB [8,9]. Chemical shift perturbation was seen at the imidazole ring NH in W8 (from 10.43 ppm to 9.73 ppm), too. The peak traces of K7 and Y15 of *Ta*-Csp which side chains form close contacts with dT_7 are shown in the box of ^{1}H–^{15}N HSQC spectra. The NMR signals gradually shifted in a single direction with the addition of dT_7, indicating that the exchange rate of dT_7 between the free and the bound states is faster than the NMR time scale.

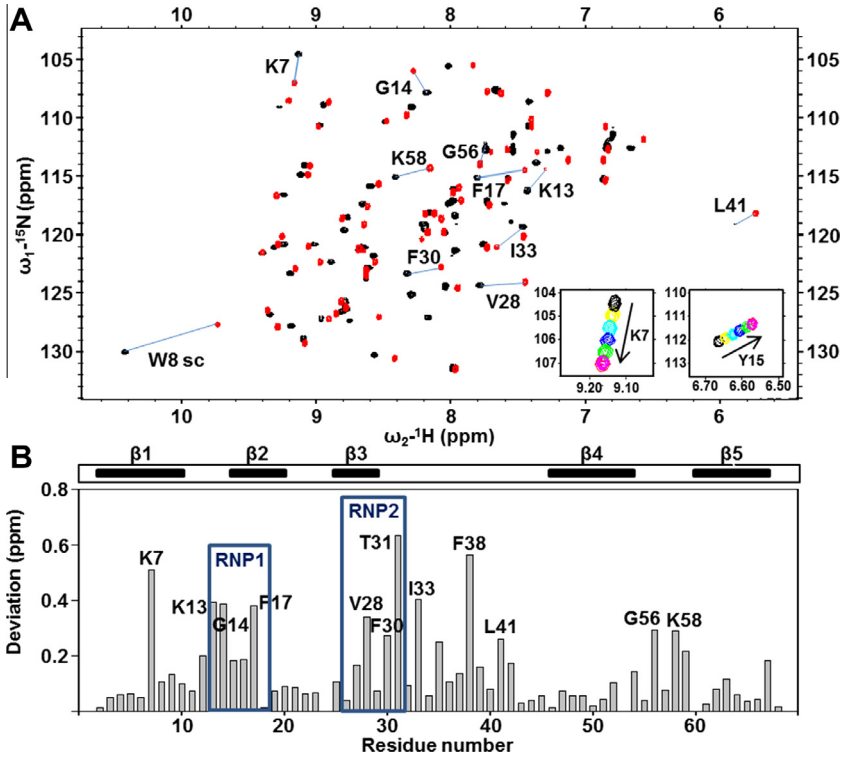

Fig. 2. (A) Overlay of ^{1}H–^{15}N HSQC spectra of free *Ta*-Csp (black) and *Ta*-Csp-dT$_7$ (red) tested at a 1:1 molar ratio of *Ta*-Csp to dT$_7$. Protein samples were prepared in 50 mM potassium phosphate buffer containing 100 mM KCl and 0.1 mM EDTA at pH 6.0. Peak traces of K7 and Y15 for the dT$_7$ titration shown in the box are the signal changes of *Ta*-Csp after titration with dT$_7$ at ratios of (a) 0:1 (black), (b) 0.1:1 (yellow), (c) 0.3:1 (sky blue), (d) 0.5:1 (blue), (e) 0.7:1 (green), (f) 1:1 (red), and (g) 1.2:1 (magenta). (B) Chemical shift perturbation upon addition of dT$_7$. Weighted average of the ^{15}N and ^{1}H chemical shift perturbations $\left(\Delta\delta = \sqrt{(\delta H^2 + 0.2(\delta N^2))}\right)$ of *Ta*-Csp upon complex formation with dT$_7$. (For interpretation of the references to colour in this figure legend, the reader is referred to the web version of this article.)

3.3.1. ^{15}N NMR relaxation study

The results of spin-relaxation experiments with free *Ta*-Csp and dT$_7$-bound *Ta*-Csp were compared and are shown in Fig. 3. The average R_1, R_2, and hNOE values of free *Ta*-Csp were 2.42 ± 0.045 s^{-1}, 6.78 ± 0.53 s^{-1}, and 0.56 ± 0.017 units, respectively; the corresponding values for dT$_7$-bound *Ta*-Csp were 2.55 ± 0.051 s^{-1}, 6.03 ± 0.21 s^{-1}, and 0.68 ± 0.027 units, respectively. The average R_2/R_1 ratio for free *Ta*-Csp was 2.80 ± 0.38, whereas that for bound *Ta*-Csp was 2.36 ± 0.15, implying that both free *Ta*-Csp and the bound form exist as monomers. Large R_2 values (>10 s^{-1}) for the backbone N-H of K7 and W8 could be due to the conformational exchange (R_{ex}) of the protein on microsecond to millisecond time scales. Conformational exchanges of K7 (10.77 → 7.77 s^{-1}), and W8 (15.47 → 6.50 s^{-1}) at the dT$_7$ binding site decreases dramatically upon binding, resulting in highly populated bound conformations.

Although there are not many structural differences between free and complex structures, the binding of dT$_7$ to *Ta*-Csp increased the hNOE values in overall structures. The average hNOE value was 0.56 for free *Ta*-Csp, which increased to 0.68 for the dT$_7$-bound form. The average hNOE values at loop regions were 0.590 (loop 1), 0.528 (loop 2), 0.513 (loop 3), and 0.487 (loop 4). The binding of dT$_7$ to *Ta*-Csp dramatically increased the hNOE values of these loop regions to 0.758, 0.573, 0.634, and 0.641, respectively. The average hNOE values at β-sheet regions also increased: 0.624 (β$_1$), 0.643 (β$_2$), 0.620 (β$_3$), 0.574 (β$_4$) and 0.585 (β$_5$). The binding of dT$_7$ to *Ta*-Csp increased the hNOE values of these regions to 0.719 (β$_1$), 0.761 (β$_2$), 0.716 (β$_3$), 0.669 (β$_4$), and 0.713 (β$_5$). Therefore, upon dT$_7$ binding, the fast time scale motions in the *Ta*-Csp structure decrease and the structure of *Ta*-Csp becomes rigid.

Microsecond to millisecond motions in *Ta*-Csp were investigated by a CPMG experiment on *Ta*-Csp and its bound form. Fig. 4A and B show the differences in R_2^{eff} values as a function of amino acid sequence, ΔR_2^{eff} (ν_{cp}), revealing that dT$_7$ binding reduced slow time scale motion, dramatically decreasing the R_{ex} values of the binding epitope and stabilizing the structure of *Ta*-Csp. In particular, the ΔR_2^{eff} values of K7 (20.19 → 7.05 s^{-1}), W8 (24.02 → 4.36 s^{-1}), Y15 (15.13 → 4.19 s^{-1}) and F17 (13.93 → 3.39 s^{-1}) dramatically decreased upon dT$_7$ binding. The relaxation dispersion data at 500 MHz NMR and 800 MHz NMR for W8 are shown in Fig. 4C. W8 located at the binding site underwent chemical exchange on a microsecond to millisecond time scale in free *Ta*-Csp, while the relaxation dispersions of these residues disappeared in dT$_7$-bound *Ta*-Csp. CPMG dispersion profiles were fit to a two-state exchange model and the rates for K7 (690 ± 55.7 s^{-1}), W8 (841 ± 67.3 s^{-1}), Y15 (616 ± 53.1 s^{-1}), and F17 (547 ± 45.2 s^{-1}) results in an average exchange rate constant of 674 ± 55.3 s^{-1} for these residues at the β1–β2 surface of the nucleic acid binding site.

4. Discussion

The three-dimensional structures and the primary sequences of Csps from psychrophilic, mesophilic, thermophilic, and hyperthermophilic bacteria are highly similar and yet the Csps exhibit a diverse range of melting points. Previously, we investigated the dynamic properties and structure of the psychrophilic *Lm*-CspA using NMR spectroscopy, and showed that *Lm*-CspA is less thermostable (~40 °C) than mesophilic Csps, and exhibits high structural flexibility [16]. The structure of *Lm*-CspA contains two salt bridges,

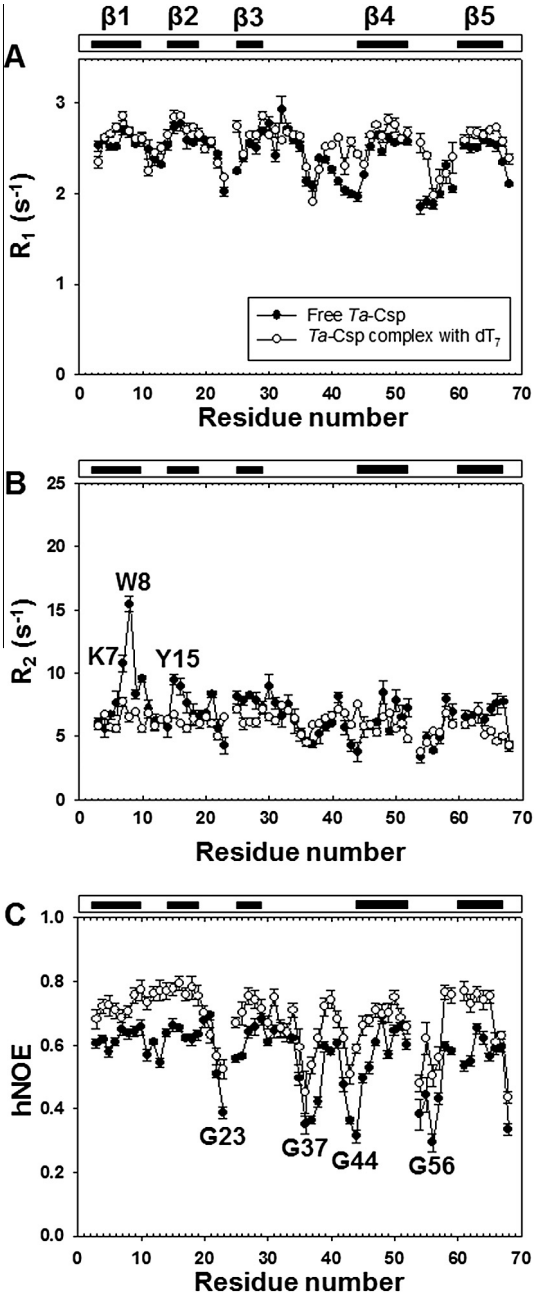

Fig. 3. Comparison of (A) R_1, (B) R_2, and (C) hNOE values for free *Ta*-Csp (filled circles) and *Ta*-Csp-dT_7 (open circles) at pH 6.0, at a molar ratio of *Ta*-Csp to dT_7 of 1:1. Solid bars represent the five β-strands of *Ta*-Csp.

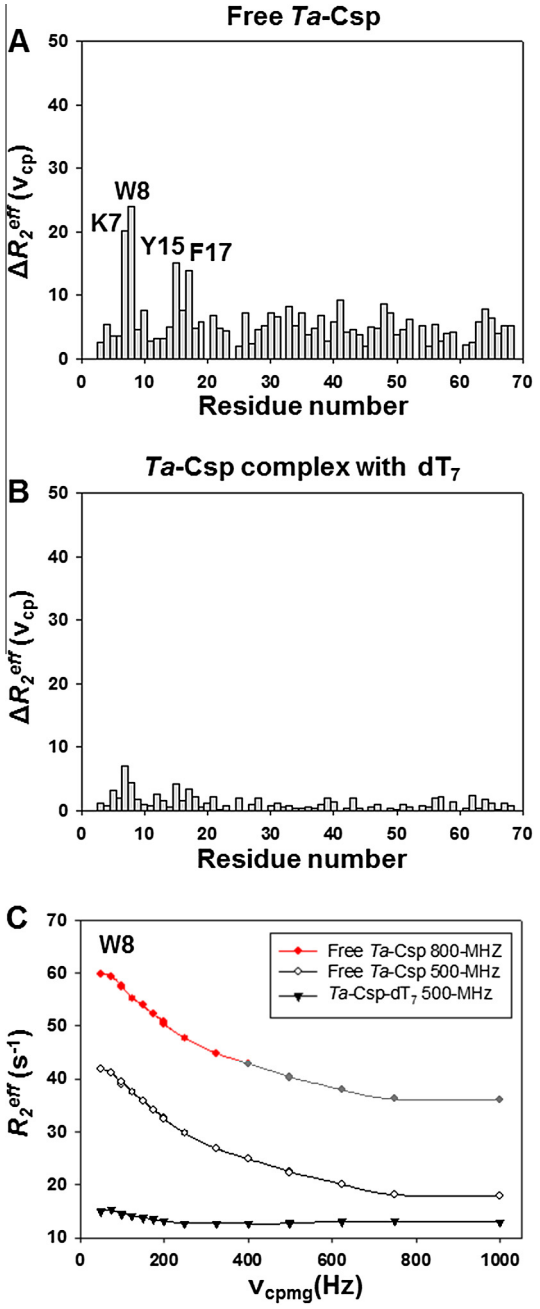

Fig. 4. Chemical exchanges in (A) free *Ta*-Csp and (B) *Ta*-Csp-dT_7. The value ΔR_2^{eff} (ν_{cp}) was determined from the difference in measured relaxation rates, R_2^{eff} (ν_{cp},50 Hz) – R_2^{eff} (ν_{cp},1000 Hz). (C) Fitted data of W8 at the nucleic acid binding site.

E2–R20 and K7–D25, and 10 hydrophobic residues (V6, F9, I18, V26, V28, L41, V47, F49, V51, and V63) forming the hydrophobic core. The mesophilic *Bs*-CspB with a T_m (~52 °C) [7] also contains two salt bridges, K7–D25 and K5–E19, but has two more hydrophobic core residues than the psychrophilic *Lm*-CspA. These hydrophobic interactions in mesophilic Csps result in a higher T_m compared to that of psychrophilic Csp. The thermophilic *Ta*-Csp with a T_m (~76 °C) includes 12 hydrophobic core residues, the same number as in mesophilic Csps. However, *Ta*-Csp has more intramolecular ion pairing (E21–K3–E48–R66, K7–D25, and K63–E52) than *Bs*-CspB, which contributes to the enhanced thermostability of *Ta*-Csp. Hyperthermophilic *Tm*-Csp with a T_m (~80 °C) has a peripheral ion cluster (D20–R2–E47–K63), two salt bridges (K6–D24 and H61–E49), and 12 hydrophobic core residues [15], similar to *Ta*-Csp. Furthermore, the thermophilic *Ta*-Csp has five β-strands—β_1 (K2–N10), β_2 (Y15–Q20), β_3 (D25–H29), β_4 (H46–G54) and β_5 (P60–R67)—like all other Csps. Compared to hyperthermophilic *Tm*-Csp, *Ta*-Csp has shorter β_2 (G13-K19) and β_3 (D24-W29) strands, resulting in longer loop 2 and loop 3. These results imply that variations in β-strand length can play a critical role in determining the thermal stability of thermophilic Csps.

Internal motions have been previously reported in ^{15}N relaxation studies of unliganded *Ec*-CspA, *Bs*-CspB, *Lm*-CspA and the *Bs*-CspB-dT_7, *Lm*-CspA-dT_7 complexes [9,16,30]. The binding of dT_7 to all Csps has been shown to reduce local dynamics and increase protein rigidity. The dT_7 binding introduces structural rigidity in the *Ta*-Csp structure, especially at the surface loop regions, as

evident by the increase in hNOE values upon dT_7 binding to *Ta*-Csp. In particular, the K13 (0.54 → 0.77) residue in loop 1 and K58 (0.60 → 0.77) residue in loop 4 showed dramatic increases in hNOE values in the dT_7-bound *Ta*-Csp compared with free *Ta*-Csp. These basic residues form contacts with the backbone phosphates of the DNA thereby contributing to the rigidity of *Ta*-Csp-dT_7 [16]. Compared to *Ta*-Csp, psychrophilic *Lm*-Csp is much more flexible and in particular loop3 is very flexible with extremely low hNOE values

In *Ta*-Csp, high ΔR_2^{eff} values for residues exclusively in the β1–β2 surface region (e.g., K7, W8, Y15, and F17) imply that this nucleic acid binding site in free *Ta*-Csp are in a dynamic equilibrium between different conformers, while other regions of the molecule display high rigidity without microseconds to milliseconds motions. In thermophilic *Ta*-Csp, salt bridges in the β4 and β5 regions (E21−K3−E48−R66 and K63−E52) connect the two strands, conflating their conformational states. In contrast, in the case of psychrophilic *Lm*-CspA, slow motions appeared in the overall structure [16]. Given that there are only two salt bridges (E2–R20 and K7–D25) between the loop regions in *Lm*-CspA, there are millisecond to microsecond time scale motions in the broader region containing the F15, F17, H29, and R56 residues [16].

In this study, we revealed the thermostability and the dynamic properties of thermophilic Csp using NMR spectroscopy for the first time. We conclude that a number of salt bridges, the length of β-strands, and hydrophobic core packing are likely key factors in determining the thermostability of *Ta*-Csp. Furthermore, spin relaxation data revealed that nucleic acid binding stabilized the native conformations of *Ta*-Csp that are found in a dynamic equilibrium in the unbound state. In a free state, aromatic rings of W8, Y15, and F17 are exposed to the solvent and is in conformational exchange between the conformers while in bound state, *Ta*-Csp has dT_7 binding stabilized the major bound conformations. ^{15}N relaxation dispersion experiments showed that slow exchange occurs only at the β1–β2 surface region with an average conformational exchange rate constant of 674 ± 55.3 s^{-1}. As shown in *Lm*-Csp, psychrophilic Csps should be more flexible to accommodate nucleic acid at extremely low temperature than thermophilic Csps. In contrast, thermophilic *Ta*-Csp has a more rigid structure and may not need high structural flexibility to accommodate nucleic acids upon cold shock.

Acknowledgments

This work was supported by the Basic Science Research Program Grant (2013R1A1A2058021) and Priority Research Centers Program Grant (2009-0093824) through the National Research Foundation of Korea, funded by the Ministry of Education, Science, and Technology.

References

[1] M.K. Shaw, J.L. Ingraham, Synthesis of macromolecules by *Escherichia coli* near the minimal temperature for growth, J. Bacteriol. 94 (1967) 157–164.
[2] M.H. Weber, M.A. Marahiel, Bacterial cold shock responses, Sci. Prog. 86 (2003) 9–75.
[3] D. Landsman, RNP-1, an RNA-binding motif is conserved in the DNA-binding cold shock domain, Nucleic Acids Res. 20 (1992) 2861–2864.
[4] D.N. Ermolenko, G.I. Makhatadze, Bacterial cold-shock proteins, Cell. Mol. Life Sci. 59 (2002) 1902–1913.
[5] K. Newkirk, W. Feng, W. Jiang, R. Tejero, S.D. Emerson, M. Inouye, G.T. Montelione, Solution NMR structure of the major cold shock protein (CspA) from *Escherichia coli*: identification of a binding epitope for DNA, Proc. Natl. Acad. Sci. USA 91 (1994) 5114–5118.
[6] H. Schindelin, W. Jiang, M. Inouye, U. Heinemann, Crystal structure of CspA, the major cold shock protein of *Escherichia coli*, Proc. Natl. Acad. Sci. USA 91 (1994) 5119–5123.
[7] A. Schnuchel, R. Wiltscheck, M. Czisch, M. Herrler, G. Willimsky, P. Graumann, M.A. Marahiel, T.A. Holak, Structure in solution of the major cold-shock protein from *Bacillus subtilis*, Nature 364 (1993) 169–171.
[8] K.E. Max, M. Zeeb, R. Bienert, J. Balbach, U. Heinemann, T-rich DNA single strands bind to a preformed site on the bacterial cold shock protein Bs-CspB, J. Mol. Biol. 360 (2006) 702–714.
[9] M. Zeeb, K.E. Max, U. Weininger, C. Low, H. Sticht, J. Balbach, Recognition of T-rich single-stranded DNA by the cold shock protein Bs-CspB in solution, Nucleic Acids Res. 34 (2006) 4561–4571.
[10] H.P. Morgan, M.A. Wear, I. McNae, M.P. Gallagher, M.D. Walkinshaw, Crystallization and X-ray structure of cold-shock protein E from *Salmonella typhimurium*, Acta Crystallogr., Sect. F: Struct. Biol. Cryst. Commun. 65 (2009) 1240–1245.
[11] G. D'Auria, C. Esposito, L. Falcigno, L. Calvanese, E. Iaccarino, A. Ruggiero, C. Pedone, E. Pedone, R. Berisio, Dynamical properties of cold shock protein A from *Mycobacterium tuberculosis*, Biochem. Biophys. Res. Commun. 402 (2010) 693–698.
[12] K.P. Gerarden, A.M. Fuchs, J.M. Koch, M.M. Mueller, D.R. Graupner, J.T. O'Rorke, C.D. Frost, H.A. Heinen, E.R. Lackner, S.J. Schoeller, P.G. House, F.C. Peterson, C.T. Veldkamp, Solution structure of the cold-shock-like protein from *Rickettsia rickettsia*, Acta Crystallogr., Sect. F: Struct. Biol. Cryst. Commun. 68 (2012) 1284–1288.
[13] K.E. Max, M. Zeeb, R. Bienert, J. Balbach, U. Heinemann, Common mode of DNA binding to cold shock domains. Crystal structure of hexathymidine bound to the domain-swapped form of a major cold shock protein from *Bacillus caldolyticus*, FEBS J. 274 (2007) 1265–1279.
[14] U. Mueller, D. Perl, F.X. Schmid, U. Heinemann, Thermal stability and atomic-resolution crystal structure of the *Bacillus caldolyticus* cold shock protein, J. Mol. Biol. 297 (2000) 975–988.
[15] W. Kremer, B. Schuler, S. Harrieder, M. Geyer, W. Gronwald, C. Welker, R. Jaenicke, H.R. Kalbitzer, Solution NMR structure of the cold-shock protein from the hyperthermophilic bacterium *Thermotoga maritima*, Eur. J. Biochem. 268 (2001) 2527–2539.
[16] J. Lee, K.W. Jeong, B. Jin, K.S. Ryu, E.H. Kim, J.H. Ahn, Y. Kim, Structural and dynamic features of cold-shock proteins of *Listeria monocytogenes*, a psychrophilic bacterium, Biochemistry 52 (2013) 2492–2504.
[17] M. Sattler, J. Schleucher, C. Griesinger, Heteronuclear multidimensional NMR experiments for the structure determination of proteins in solution employing pulsed field gradients, Prog. Nucl. Magn. Reson. Spectrosc. 34 (1999) 93–158.
[18] J.P. Simorre, B. Brutscher, M.S. Caffrey, D. Marion, Assignment of NMR spectra of proteins using triple-resonance two-dimensional experiments, J. Biomol. NMR 4 (1994) 325–333.
[19] G.W. Vuister, T. Yamazaki, D.A. Torchia, A. Bax, Measurement of two- and three-bond ^{13}C–^{1}H J couplings to the C delta carbons of leucine residues in staphylococcal nuclease, J. Biomol. NMR 3 (1993) 297–306.
[20] F. Delaglio, S. Grzesiek, G.W. Vuister, G. Zhu, J. Pfeifer, A. Bax, NMRPipe: a multidimensional spectral processing system based on UNIX pipes, J. Biomol. NMR 6 (1995) 277–293.
[21] What's Sparky Anderson got to do with health care?, Health Law Vigil 9 (1986) 5–6.
[22] P. Guntert, K. Wuthrich, Improved efficiency of protein structure calculations from NMR data using the program DIANA with redundant dihedral angle constraints, J. Biomol. NMR 1 (1991) 447–456.
[23] G. Cornilescu, F. Delaglio, A. Bax, Protein backbone angle restraints from searching a database for chemical shift and sequence homology, J. Biomol. NMR 13 (1999) 289–302.
[24] J. Kordel, N.J. Skelton, M. Akke, A.G. Palmer 3rd, W.J. Chazin, Backbone dynamics of calcium-loaded calbindin D9k studied by two-dimensional proton-detected 15N NMR spectroscopy, Biochemistry 31 (1992) 4856–4866.
[25] K.W. Jeong, J.Y. Lee, S.A. Lee, S.P. Yang, H. Ko, D.I. Kang, C.B. Chae, Y. Kim, Dynamics of a heparin-binding domain of VEGF(165) complexed with its inhibitor triamterene, Biochemistry 50 (2011) 4843–4854.
[26] K.W. Jeong, M.C. Jeong, B. Jin, Y. Kim, Relationship between structural flexibility and function in the C-terminal region of the heparin-binding domain of VEGF(165), Biochemistry 52 (2013) 8823–8832.
[27] M. Tollinger, N.R. Skrynnikov, F.A.A. Mulder, J.D. Forman-Kay, L.E. Kay, Slow dynamics in folded and unfolded states of an SH3 domain, J. Am. Chem. Soc. 123 (2001) 11341–11352.
[28] F.A. Mulder, N.R. Skrynnikov, B. Hon, F.W. Dahlquist, L.E. Kay, Measurement of slow (micros-ms) time scale dynamics in protein side chains by (15)N relaxation dispersion NMR spectroscopy: application to Asn and Gln residues in a cavity mutant of T4 lysozyme, J. Am. Chem. Soc. 123 (2001) 967–975.
[29] G.I. Makhatadze, V.V. Loladze, A.V. Gribenko, M.M. Lopez, Mechanism of thermostabilization in a designed cold shock protein with optimized surface electrostatic interactions, J. Mol. Biol. 336 (2004) 929–942.
[30] W. Feng, R. Tejero, D.E. Zimmerman, M. Inouye, G.T. Montelione, Solution NMR structure and backbone dynamics of the major cold-shock protein (CspA) from *Escherichia coli*: evidence for conformational dynamics in the single-stranded RNA-binding site, Biochemistry 37 (1998) 10881–10896.